THIRD QUARTERLY REPORT

FOR

A DAY-NIGHT HIGH RESOLUTION INFRARED RADIOMETER EMPLOYING TWO-STAGE RADIANT COOLING

(1 October 1966 - 1 January 1967)

Contract No. NAS 5-10113

Prepared by

ITT Industrial Laboratories
Fort Wayne, Indiana 46803

For

National Aeronautics and Space Administration
Goddard Space Flight Center
Greenbelt, Maryland 20771

ITTIL No. 67-1002 15 January 1967

THIRD QUARTERLY REPORT

FOR

A DAY-NIGHT HIGH RESOLUTION INFRARED RADIOMETER EMPLOYING TWO-STAGE RADIANT COOLING

(1 October 1966 - 1 January 1967)

Contract No. NAS 5-10113

Prepared by

ITT Industrial Laboratories
Fort Wayne, Indiana 46803

For

National Aeronautics and Space Administration
Goddard Space Flight Center
Greenbelt, Maryland 20771

Contributors

R. V. Annable, J. F. Lodder,
D. J. Juarez, R. A. Harber

Approved by

K. L. DeBrosse, Manager
Space & Applied Science Dept.

C. W. Steeg Jr., Director
Product Development

R. T. Watson, President
ITT Industrial Laboratories

ABSTRACT

This report covers the continuation of design and construction of a two-stage radiant cooler to be used in a 10.5 to 12.5 micron Day-Night High Resolution Infrared Radiometer. It contains descriptions of the outer box and first-stage cone construction and the second-stage design. The design of test equipment for simulating cold space is outlined. The effects of patch thickness and altitude of operation on cooler geometry are studied, and the joule heating of the detector investigated. Finally, additional optical design and initial electronic design are covered.

TABLE OF CONTENTS

LIST OF ILLUSTRATIONS

LIST OF TABLES

1.0 INTRODUCTION

This report covers the continuation of design and construction of a two-stage radiant cooler to be used in cooling an infrared detector in a 10.5 to 12.5 micron day-night radiometer. During the reporting period the outer box and cone for a single-stage thermal test model were constructed and the second-stage cone and patch designed. The design of a cold space simulator was completed. The effects of patch thickness and lower altitude operation on cooler design were investigated, and the effect of joule heating of the detector studied. Additional optical design was carried out and electronic design of input circuitry begun.

A 10.5 to 12.5 micron instrument permits radiometric mapping of the earth and its cloud cover both day and night. It is an extension of the 3.4 to 4.2 micron nighttime High Resolution Infrared Radiometer flown on Nimbus I and II. The two-stage radiant cooler is an extension of the single-stage cooler employed on the Nimbus radiometer.

This report is for the second quarter of the second phase of the program, which was initiated following approval of the First Quarterly (Design Study) Report on 24 June, 1966. The second phase is the construction and testing of a vibrationally sound two-stage cooler, with the objective of attaining a temperature below 80 degrees K. The third phase is the integration of the radiant cooler with a working breadboard radiometer of specific characteristics.

2.0 MECHANICAL DESIGN AND CONSTRUCTION

The construction of a single-stage model of the radiant cooler is nearly finished, and the mechanical design of the second stage has been completed.

2.1 Construction of Single-Stage Model

One first-stage cone and outer box have been completed (Figures 1, 2 and 3). The patch for the assembly of a single-stage model will be ready in the first part of the next quarter. Most of the cone and box parts are fitted on assembly and reworked to fit as necessary; this eliminates fabrication of special fixtures.

Rigid sheets of urethane foam were purchased from Pittsburgh Corning Corp. for the core material in the panels. These sheets were sliced to desired thickness and cut into 12 inch by 12 inch square blocks. They were then cemented between the aluminum sheets with silicone adhesive. The cone assembly, shown in Figures 1, 2 and 3, has the gold deposited on top of an aluminized epoxy film.

Parts are also available for a second cone assembly with gold evaporated over aluminized Alzak treated aluminum. The surfaces are evaporated with aluminum to increase adherence of the gold coating. A third cone assembly will have 0.010 inch mylar bonded to its inner surface. The mylar will then be aluminized and gold coated. We are presently investigating bonding methods to obtain a smooth surface between the mylar and aluminum alloy skin.

2.2 Design of Second-Stage Cone and Patch

Figure 4 shows the second-stage cone and patch mounted to the first-stage patch. The second-stage cone is molded in two halves from rigid polyurethane foam and coated with epoxy and gold on all sides. Mounting brackets of aluminum sheet allow the cone to be assembled to the first-stage patch after installation of the second-stage patch. The second-stage patch is machined from 6061-T6 aluminum and contains a cavity for mounting the detector cell housing (Figure 5). The Synthane G-10 support tube for the patch has a spherical mount which can be used to center the detector element on the optic axis and then be locked in place. The interference filter and aplanatic lens are mounted in a stainless steel tube potted in place in the first-stage patch. A fixture is used to center the tube on the optic axis during potting with urethane foam.

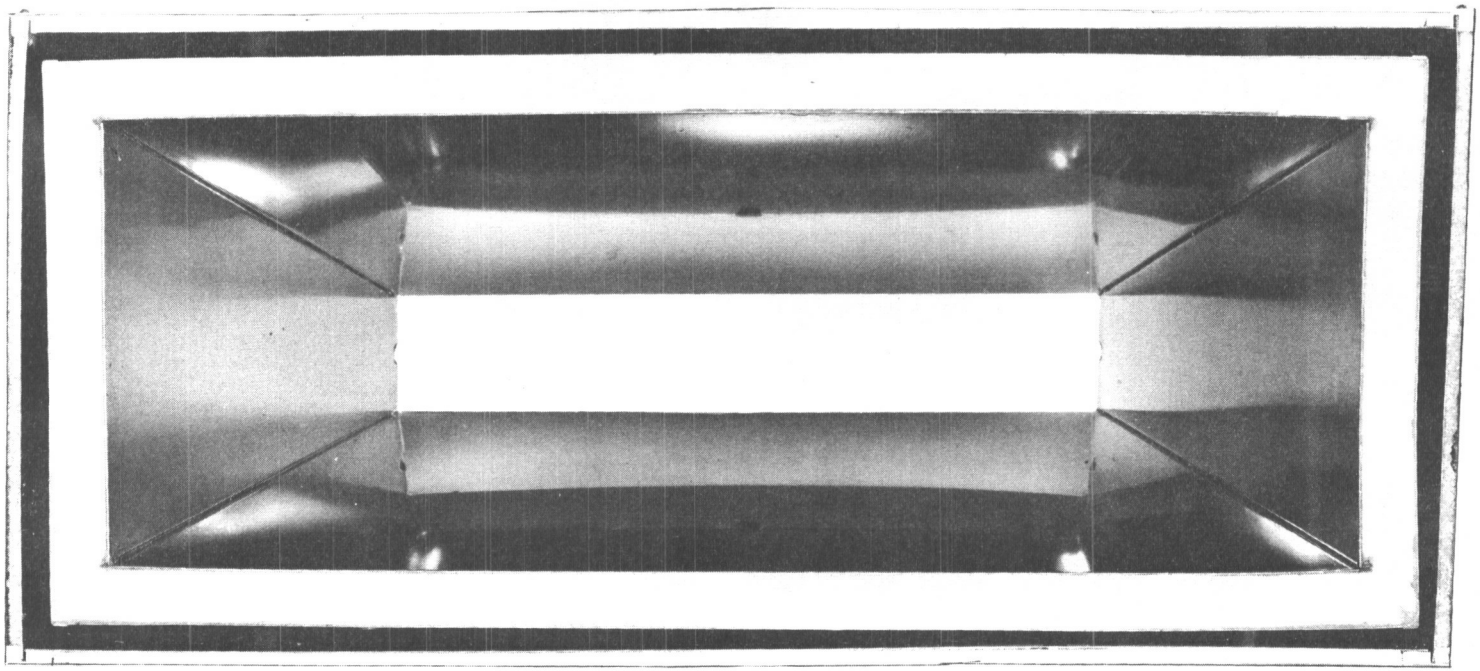

Figure 1 First-Stage Cone Mounted in Outer Box, Front View

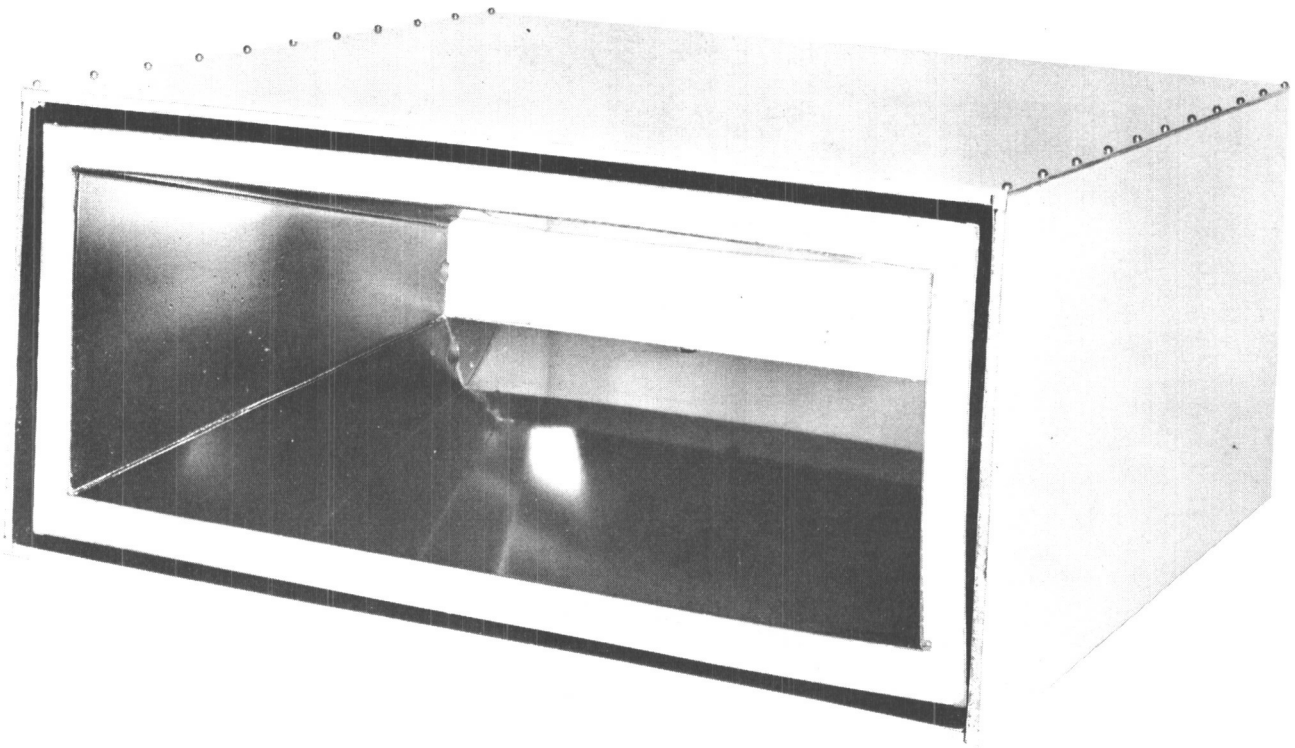

Figure 2 First-Stage Cone Mounted in Outer Box, Oblique View

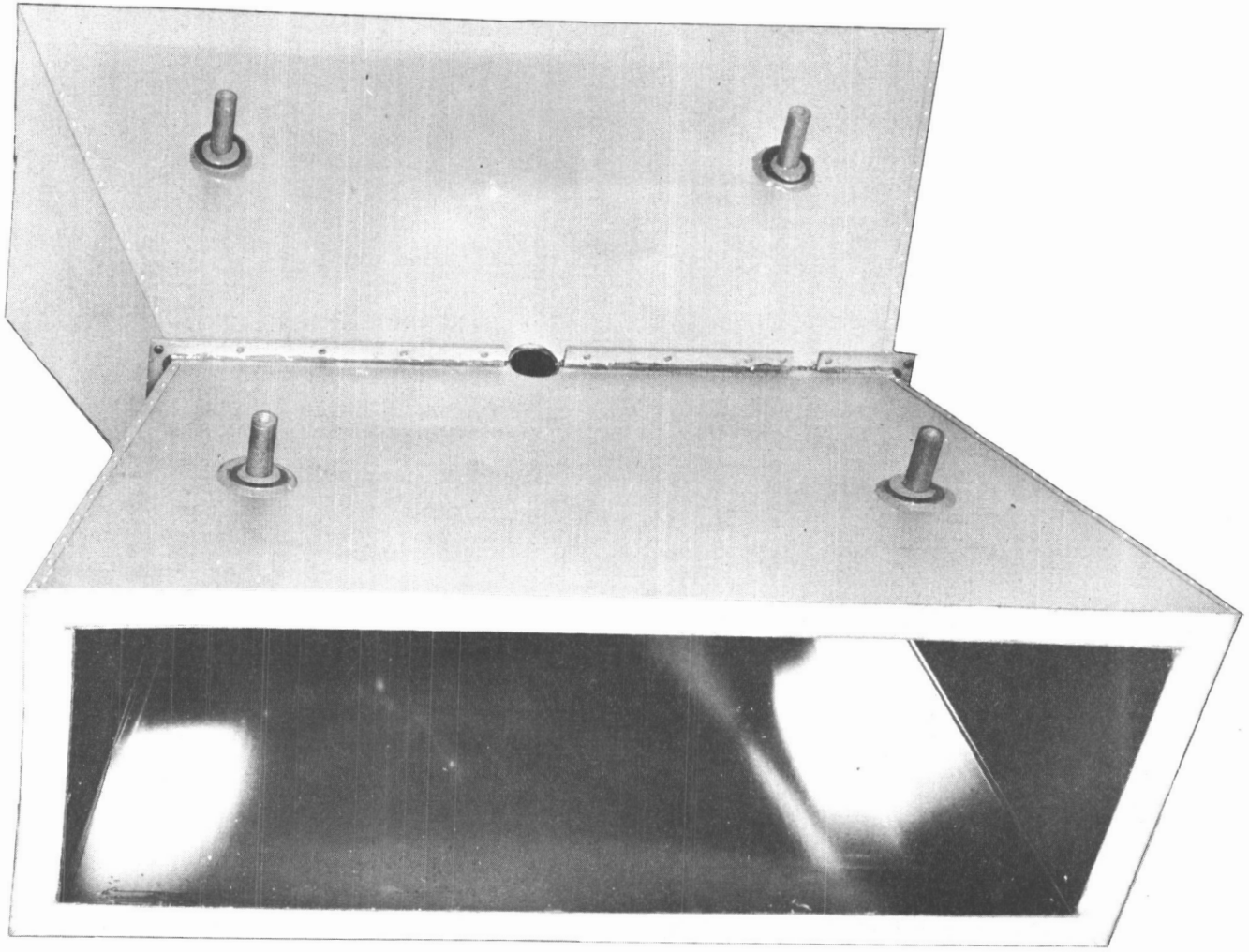

Figure 3 First Stage Cone

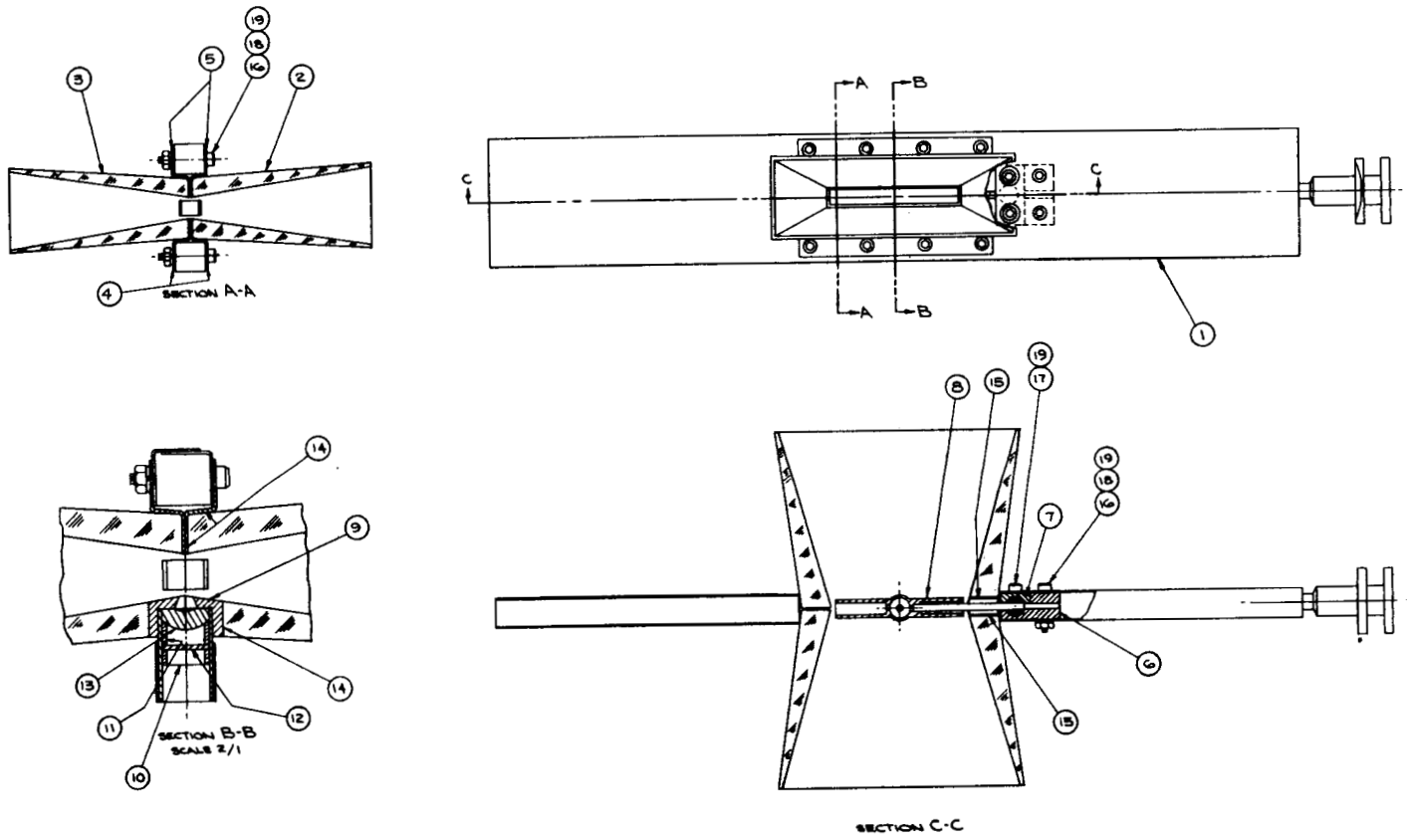

Figure 4 First and Second Stage Patch Assembly

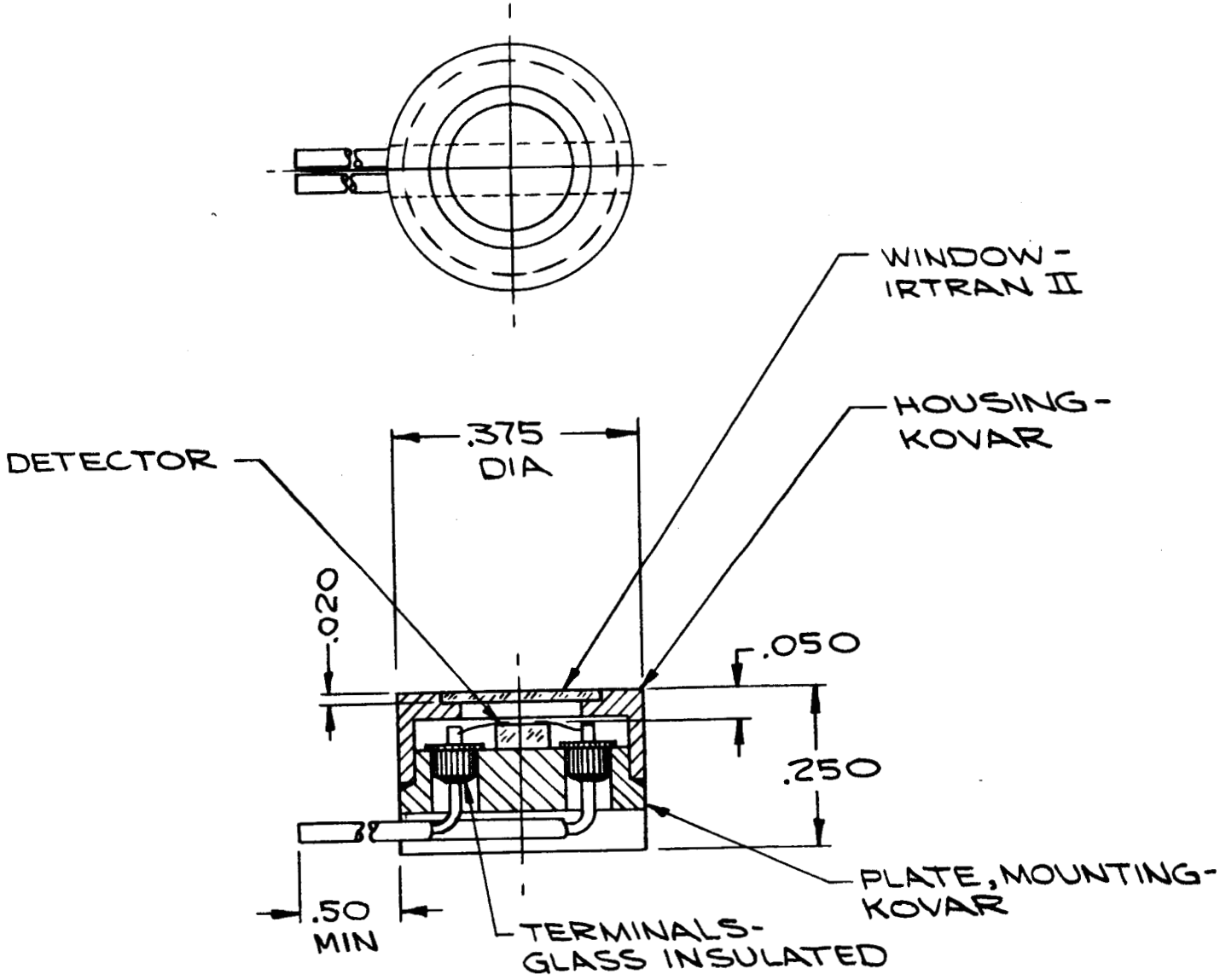

Figure 5 Detector Assembly

3.0 TEST EQUIPMENT

The second cold exchanger of a helium refrigerator (cryogenerator) will cool a copper target used to simulate cold space (First Quarterly Report, Section 5.1). The copper target will be shielded from ambient radiation by an aluminum shroud cooled by the intermediate cold exchanger of the helium refrigerator. Both the target and shroud will be suspended in the space chamber as shown in Figure 6. The cable suspensions conduct a negligible amount of power from the space chamber to the copper target and aluminum shroud (Appendix III).

In designing the cold target and shroud for the two-stage radiant cooler particular attention was given to the connection between the target and the cryogenerator. The cold target must not be mounted in any manner which can cause significant mechanical loading on the cold head; this could result in high bending stresses due to vibration and thermal contraction and would damage the cold head. The suspensions system, shown in Figure 6, will be used to support the copper target and aluminum shroud. This suspension will carry the total weight (~ 184 pounds) of the cold target in a manner which will distribute the static weight equally about the system's center of gravity. Stainless steel cables with adjustable lengths will be attached to a stainless steel frame fastened to the inside surface of the space chamber. The weight of the cold target will be transferred from the cables to the frame through compression springs which will dampen any vibration and will also provide for the change in length produced by thermal contractions. With the rigid coupling between the cold target and cryogenerator, only about 17 pounds of loading will be present on the cold head after thermal contraction. This is the force necessary to elongate the springs an amount equal to the thermal shrinkage in the mechanical couplings when their temperature is reduced from ambient to -250 degrees F (16 degrees K).

The materials necessary for fabrication of the suspended cold target and aluminum shroud assemblies are on hand. The assemblies will be fitted in the space chamber after its installation.

A welded steel platform for the cryogenerator was designed and fabricated (Figure 7). The cryogenerator will be mated to the space chamber by raising the platform on jacks (First Quarterly Report, Section 5.1).

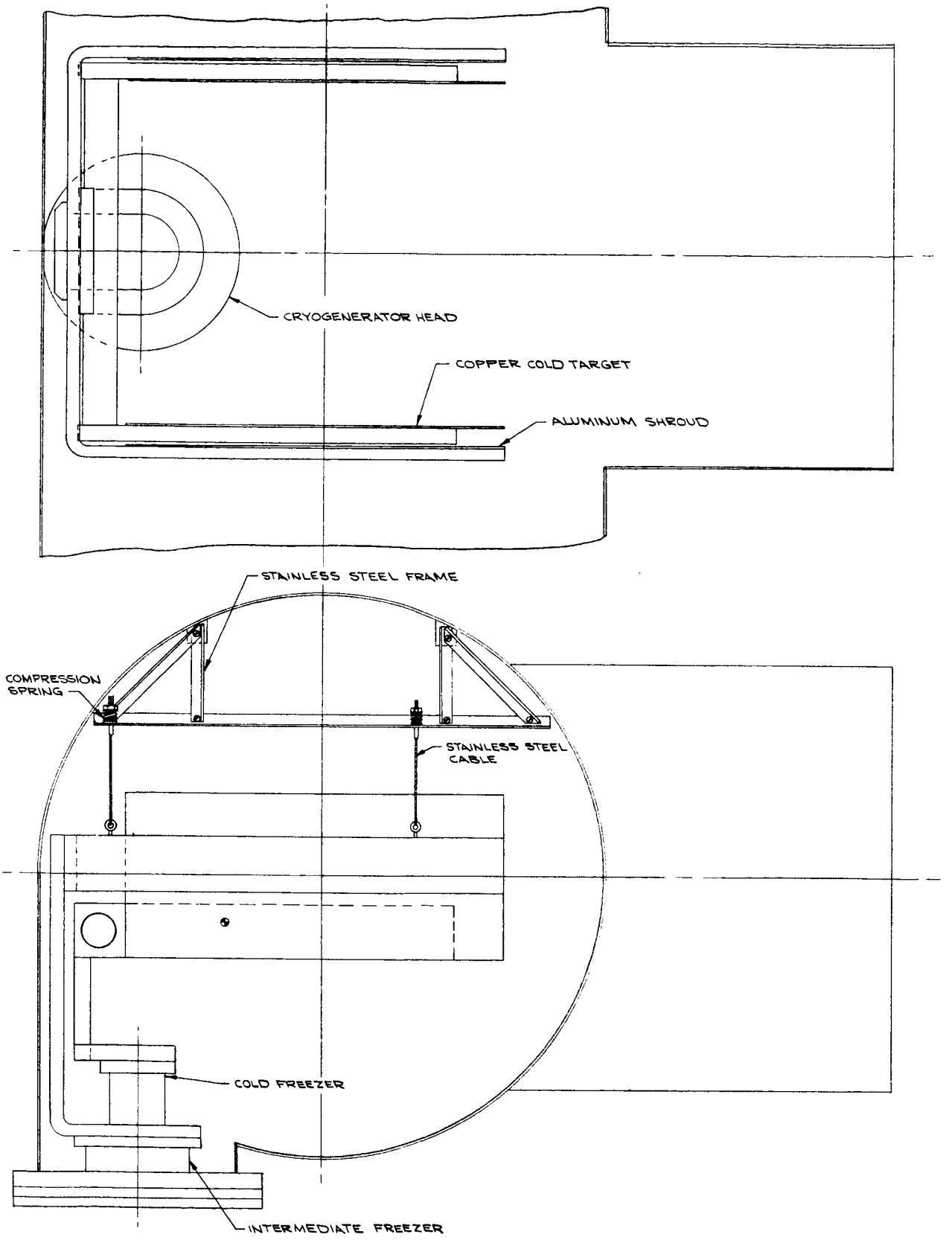

Figure 6 Suspension of Cold Target and Shroud in Space Chamber

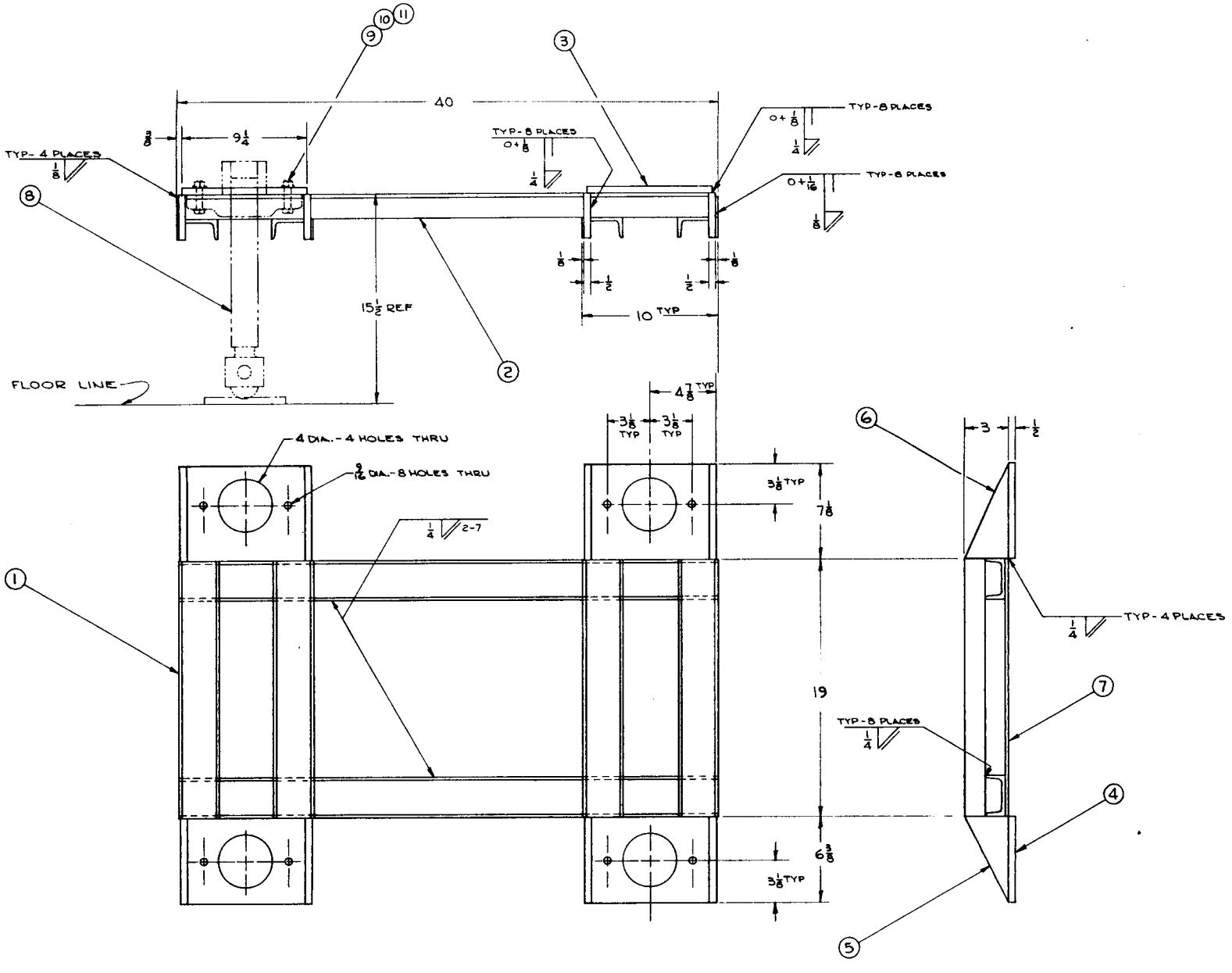

Figure 7 Cryogenerator Platform

4.0 THERMAL DESIGN

The use of patches with non-zero thicknesses increases the view factors above the original design values (First Quarterly Report, Section 3.2 and Appendix VI). This change combined with operation at a minimum altitude of 500 nautical miles requires changes in the vertical plane design of the radiant cooler.

The radiant power levels of the two stages are important in determining the thermal effect of electrical and optical inputs to the cooler and in guiding the design of electronic circuitry. The ranges of power levels were calculated for the original design modified by the non-zero patch thicknesses (minimum altitude of 650 nautical miles).

4.1 Effect of Patch Thickness on View Angles

The non-zero thickness of the radiant patch produces small changes in the view angles and view factors in both stages of the radiant cooler. In the first stage, the maximum view angle is increased slightly in both the vertical and horizontal planes. In the second stage, the view factor from the patch to the first-stage cone is increased.

The first-stage patch has a thickness of 1/2 inch; this increases the maximum view angle from the patch normal to 32.7 degrees in the vertical plane and 60.7 degrees in the horizontal. The original design values were 31.5 degrees and 60 degrees, respectively (First Quarterly Report, Section 3.2 and 3.3). The angle between the patch normal and the tangent line to the earth in the vertical plane is about 32.7 degrees at a spacecraft altitude of 650 nautical miles (31.5 degrees corresponds to about 600 nautical miles). To preserve the maximum look angles at 31.5 degrees and 60.0 degrees, the total cooler length would have to be increased by 1.6 inches, to 22.3 inches (see Section 4.2 for a discussion of 500 nautical mile design).

The second-stage patch has a thickness of 5/16 inch; this exposes the edge of the patch in the horizontal plane to a direct view from the first-stage cone and increases the view factor to the first-stage cone from the center of the patch. The total (mouth to mouth) length of the second-stage cone was increased from 5.94 inches to 6.04 inches to eliminate the direct look. The view factor to the first-stage cone from the center of the patch was then calculated at the increased cone length for both the horizontal and vertical plane geometries. The average view factor from the second-stage patch to the first-stage cone is now 2.85×10^{-2} compared with the previous value of 1.36×10^{-2} (First Quarterly Report, Appendix VI).

4.1.1 First Stage

The maximum look angles of the first-stage patch for a non-zero patch thickness may be determined by assuming the cone length (distance from patch to cone along patch normal) is reduced by half the patch thickness, as shown in Figure 8. From Appendix I to the First Quarterly Report, the maximum look angle ϕ is then given by

$$\sin(\phi - \theta) = \frac{1}{1 + \frac{\ell}{C} \tan\theta} \qquad (1)$$

where

θ = half angle of cone

C = half width of patch

ℓ = cone length

Note that the patch half width as used in the equation extends to the surface of the cone (Figure 8). For a patch 1/2 inch thick in a cone 10.35 inches long, we have

$$\ell = 10.35 - 0.25 = 10.10 \text{ inches}$$

In the vertical plane,

$$\theta_V = 13.5 \text{ degrees}$$

$$2C_V = 2.25 + 1/2 \tan 13.5 \text{ degrees} = 2.37 \text{ inches}$$

The maximum look angle from patch normal is therefore increased to

$$\phi_V = 32.7 \text{ degrees}$$

The angle ϕ_t between the patch normal and the tangent to the earth in the vertical plane is given in Table 1 for various satellite altitudes h in nautical miles.

Table 1
Angle to Earth as Function of Altitude

h	ϕ_t
600	31° 37.5'
650	32° 45'
700	33° 48'
750	34° 49'

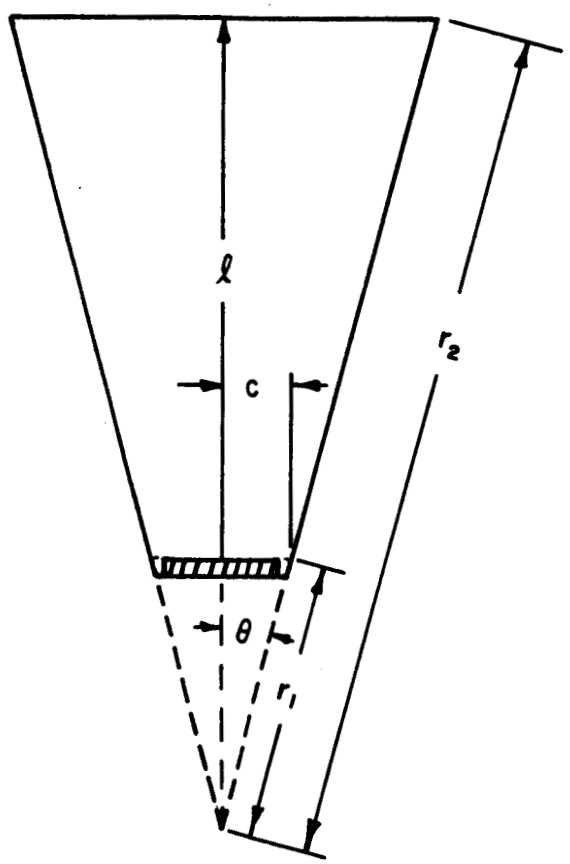

Figure 8 Cone Geometry for Patch of Non-Zero Thickness

The maximum vertical look angle of 32.7 degrees therefore corresponds to a spacecraft altitude of about 650 nautical miles.

In the horizontal plane,

$$\theta_H = 18 \text{ degrees}$$

$$2C_H = 13.70 + 1/2 \tan 18 \text{ degrees} = 13.8625 \text{ inches}$$

The maximum look angle from the patch normal is

$$\phi_H = 60.7 \text{ degrees}$$

In order to preserve the maximum look angle at its original value, we must preserve the original ℓ/C ratio when the cone half angle is fixed In the vertical plane, the cone length required for a maximum look angle of 31.5 degrees is therefore

$$\ell_v = \frac{2.37}{2.27} \times 10.35 = 10.90 \text{ inches}$$

And in the horizontal plane, the cone length required for a maximum look angle of 60 degrees is, for a spherical patch.

$$\ell_h = \frac{13.8625}{13.70} \times 10.35 = 10.48 \text{ inches}$$

For a 1/2-inch thick flat patch, the maximum horizontal look angle is 59.5 degrees. The spherical patch formula, however, gives a very good approximation in the vertical plane. The vertical plane therefore requires a longer cone. For a 1/2-inch thick patch, the total cooler length is then $2 \times 10.9 + 0.5 = 22.3$ inches, an increase of 1.6 inches.

4.1.2 Second Stage

A non-zero patch thickness in the second stage produces a direct view of the first-stage cone from the patch edge in the horizontal plane and increases the view factor to the first-stage cone from the patch center. The length of the second-stage cone was therefore increased to eliminate the direct view of the first-stage cone and the view factor to the first-stage cone determined for the new cone length. The patch thickness was assumed to be 0.32 inch (i.e., slightly more than 5/16 inch).

The procedure used to determine the new cone length can be explained by reference to Figure 9. The angle η_e is the angle at the patch edge in the horizontal plane from the patch normal to the line from the patch edge to the farther end of the first-stage cone. The angle ψ_e is from the patch normal to the line from the patch edge to the farther end of the second-stage cone. To eliminate the direct view to

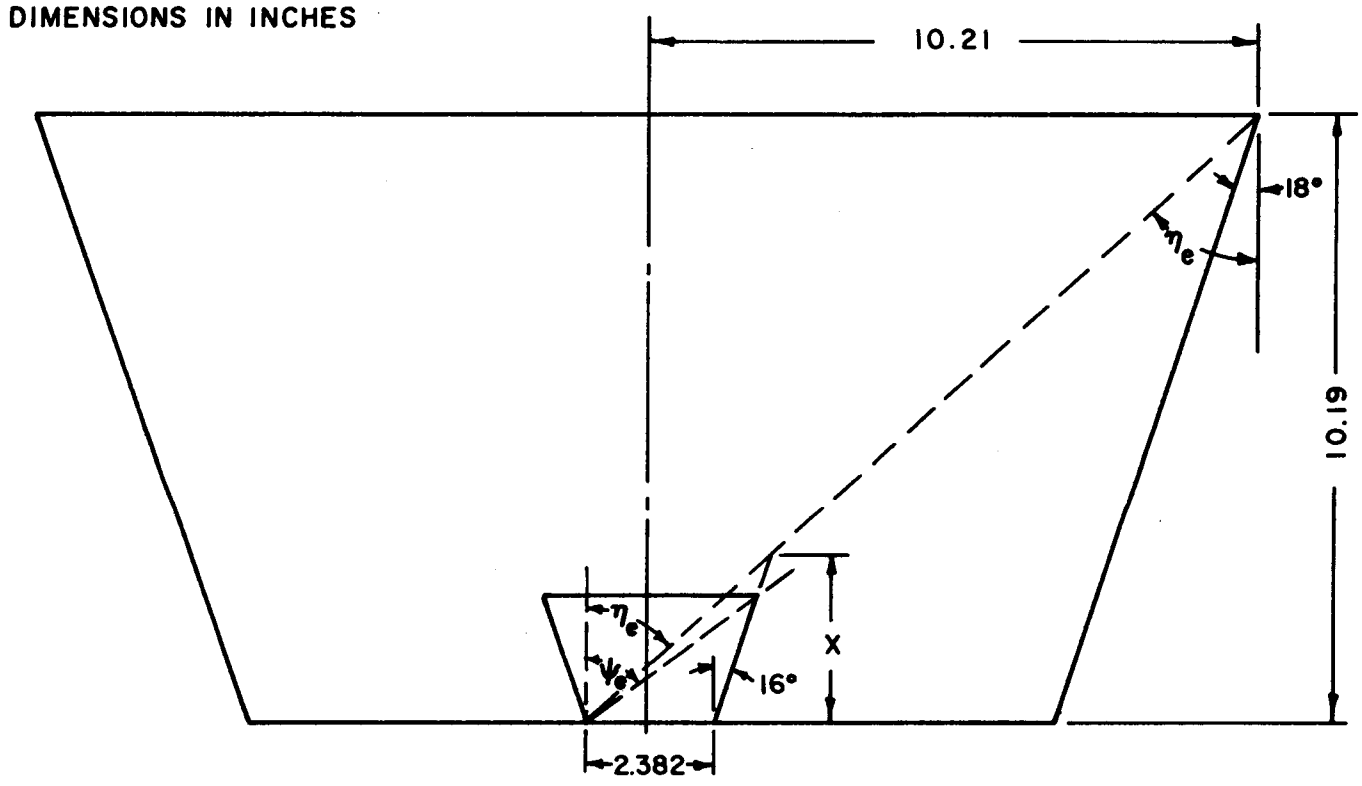

Figure 9 Determination of Length For Second-Stage Cone

the first-stage cone, the length, X, of the second-stage cone (measured from the top of the second-stage patch) must be increased until ψ_e equals η_e. In Figure 9, the length of the first-stage cone (10.19 inches) is also measured from the top of the second-stage patch (i.e., the original length is reduced by half the thickness of the second-stage patch).

From Figure 9, we have

$$\tan \eta_e = \frac{11.40}{10.19} = 1.119$$

Elimination of the direct look requires

$$\tan \psi_e = \frac{2.382 + X \tan 16 \text{ degrees}}{X} = 1.119$$

$$X = 2.86 \text{ inches}$$

The cone length (distance from patch to cone mouth along patch normal) was 2.97 inches (Second Quarterly Report, Section 2.0) for a patch of zero thickness. The new cone length measured for a zero patch thickness is

$$\ell_2 = X + 0.16 = 3.02 \text{ inches}$$

or an increase of 0.05 inch.

The view factor from the center of the second-stage patch to the first-stage cone was then calculated in the vertical and horizontal planes for an effective cone length of X = 2.86 inches. This was done using the procedure described in Appendix VI to the First Quarterly Report (See Appendix III to the Second Quarterly Report for corrections to equations VI-1 through VI-5). The parameters of interest are

$\ell^{(1)}$ = cone length in the first-stage

r_1 = distance along cone from apex to top of patch in second stage

r_2 = distance along cone from apex to cone mouth in second stage

θ = half angle of second-stage cone

b = half width of first-stage cone mouth

The effective patch widths are

$2C_V = 0.404$ inch

$2C_H = 2.382$ inches

in the vertical and horizontal planes, respectively, of the second stage. The values of r_1 and r_2 can then be calculated from

$$r_1 = \frac{c}{\sin \theta} \qquad (2)$$

$$(r_2 - r_1) \cos \theta = 2.86 \text{ inches}$$

The cone length of the first stage to be used in the calculations is the cone length for a first-stage patch of zero thickness minus one-half the second-stage patch thickness, or

$$\ell^{(1)} = 10.35 - 0.16 = 10.19 \text{ inches}$$

The values of b are

$$b_V = 3.61 \text{ inches}$$

$$b_H = 10.21 \text{ inches}$$

The partial view factors, $F^{(n)}_{p2\text{-}c1}$ were then determined for $\theta_V = 9$ degrees and $\theta_H = 16$ degrees (equation VI-6, Appendix VI to the First Quarterly Report). The results are given in Table 2.

Table 2
Partial View Factors for Non-Zero Patch Thickness

n	vertical			horizontal		
	ψ_n	η_n	$F^{(n)}_{p2\text{-}C1}$	ψ_n	η_n	$F^{(n)}_{p2\text{-}c1}$
1	37^o 40'	39^o 7'	0	82^o 18'	80^o 47.5'	0.00875
2	60^o 20'	58^o 32'	0.0257	90^o	90^o	0
3	80^o 4'	77^o 57'	0.0154			
4	90^o	85^o 9'	0.0072			
		$F_{p2\text{-}c1}$ =	0.0483		$F_{p2\text{-}c1}$ =	0.00875

Note that for ψ_n less than or equal to η_n the partial view factor is zero. The average value of the view factor from the center of the second-stage patch to the first-stage cone is 2.85×10^{-2}, compared to the previous value of 1.36×10^{-2} (First Quarterly Report, p. VI-5).

The radiative coupling power between the second-stage patch and first-stage cone expressed as a fraction of second-stage total patch power is (First Quarterly Report, equation VI-9).

$$\frac{\Phi_{p2\text{-}c1}}{\Phi_{p2}} = \epsilon_g \, F_{p2\text{-}c1} \left(\frac{T_{c1}}{T_{p2}} \right)^4 \tag{3}$$

where

ϵ_g = emissivity of gold on first-stage cone

T_{c1} = temperature of first-stage cone

T_{p2} = temperature of second-stage cone

For

ϵ_g = 0.086

T_{c1} = 199 degrees F

T_{p2} = 79 degrees K

We obtain

$$\frac{\Phi_{p2 - c1}}{\Phi_{p2}} = 9.87 \times 10^{-2} \tag{4}$$

This would increase the patch temperature by about 2.5 percent or 2.0 degrees K.

4.2 Design for 500 Nautical Mile Altitude

The two-stage radiant cooler may fly on a spacecraft which has a minimum altitude of 500 nautical miles. The original design was for a 600 nautical mile minimum altitude (First Quarterly Report, Section 3.2). The addition of a 1/2 thick first-stage patch increased it to 650 nautical miles (Section 4.1). The maximum patch look angle must therefore be reduced in the vertical plane so the patch does not see the earth from 500 nautical miles. At this altitude, the angle from the patch normal to the tangent line to the earth is 29.2 degrees in the vertical plane. The first-stage patch will therefore be redesigned for a maximum vertical look angle of 29.0 degrees. The design of the initial thermal test module will not be changed however. The final design will be set after the important radiative transfer parameters have been determined (First Quarterly Report, Section 5.4.).

The angles and dimensions in the horizontal plane will not be changed. The maximum look angle in the horizontal plane for a 1/2-inch thick flat (rather than spherical) patch is 59.5 degrees from the patch normal. The first-stage cone angle in the vertical plane will also be kept the same. As shown in Table 3, the ratio of cone length to patch half-width is increased by less than 0.5 percent if the cone angle is kept at 13.5 degrees instead of changed to the optimum value of 12.5 degrees.

Table 3
Cone Length to Patch Half-Width as Function of Cone Angle

Vertical Plane

Cone Angle	Cone Length/Patch Half Width
12^{o} 0'	11.387
12^{o} 15'	11.376
12^{o} 30'	11.371
12^{o} 45'	11.374
13^{o} 0'	11.383
13^{o} 15'	11.399
13^{o} 30'	11.421

Because it is not desirable to increase the cone length, the maximum look angle of 29.0 degrees in the vertical plane will be obtained by reducing the width of the first-stage patch. For a cone length (distance from top of patch to cone mouth along patch normal) of 10.10 inches and a cone angle of 13.5 degrees, the width of the cone at the top of the patch is

$$\frac{10.10}{1/2 \times 11.421} = 1.769 \text{ inches}$$

For a patch 1/2 inch thick, the width of the cone at the middle of the cooler is then

$$1.769 - 1/2 \tan 13.5 \text{ degrees} = 1.652 \text{ inches}$$

Allowing a clearance of 0.065 inch between the patch and cone, the actual patch width is 1.52 inches (reduced from 2.10 inches). The patch length will be its present value of 13.56 inches.

The design of the second stage will not be changed. The patch dimensions in the second stage are already about as small as desirable for construction and alignment. The decrease in first-stage patch width reduces the cone mouth width by the same amount and increases the view factor from the second-stage patch to the first-stage cone in the vertical plane. Because of the geometry involved, a relatively large increase in the total length of the second-stage cone (from about 6 to 6.9 inches) is required to maintain the view factor (Section 4.1). Moreover, an increase in the length of the second-stage cone increases loading on the first stage (second-stage cone) from the first-stage cone and from external sources beyond the maximum look angle of the first-stage patch (First Quarterly Report, Section 3.4).

The partial view factors, $F_{p2-c1}^{(n)}$, from the second-stage patch to the first-stage cone are given in Table 4 for the reduced first-stage patch width (500 nautical mile design).

Table 4
Partial View Factors for 500 Nautical Mile Design

	vertical			horizontal		
n	ψ_n	η_n	$F_{p2-c1}^{(n)}$	ψ_n	η_n	$F_{p2-c1}^{(n)}$
1	37^o 40'	37^o 53'	0	82^o 18'	80^o 47.5'	0.00875
2	60^o 20'	57^o 9'	0.0490			
3	80^o 4'	75^o 56'	0.0316			
4	90^o	84^o 30'	0.0092			

The angles ψ_n subtended by the second-stage cone reflected in itself are unchanged from those given in Section 4.1.

The radiative coupling power to the second-stage patch from the first-stage cone expressed as a fraction of the second-stage total patch power is

$$\frac{\Phi_{p2-C1}}{\Phi_{p2}} = \epsilon_g \left(\frac{T_{c1}}{T_{p2}}\right)^4 F'_{p2-c1} \qquad (5)$$

where

ϵ_g = emissivity of gold coatings

T_{c1} = temperature of first-stage cone

T_{p2} = temperature of second-stage patch

$$F'_{p2\text{-}c1} = \frac{1}{2}\left[\sum_{\text{vertical}}^{n} \rho g \, F_{p2\text{-}c1}^{(n)} + \sum_{\text{horizontal}}^{n} \rho g \, F_{p2\text{-}c1}^{(n)}\right] \quad (6)$$

$\rho g = 1 - \epsilon_g$ = gold infrared reflectivity

This equation more accurately describes the power ratio than the formula given in the First Quarterly Report (equation VI-9) and used in Section 4.1, since it includes reflection losses within the second-stage cone.

For ϵ_g = 0.086

T_{c1} = 199 degrees K

T_{p2} = 79 degrees K

and the above values of partial view factors, we obtain

$$\frac{\Phi_{p2\text{-}c1}}{\Phi_{p2}} = 13.8 \times 10^{-2} \quad (7)$$

This would increase the patch temperature by about 3.4 percent or 2.7 degrees K.

4.3 Radiant Power Level of Patches

The actual power levels radiated by the patches are important in determining the influence of nonscaling (fixed) thermal inputs to the patches and in setting the allowable joule heating of the detector element. The fixed thermal inputs are conductive by way of the electrical leads and radiative by way of the optical openings to the detector (First Quarterly Report, Section 3.1). In addition, the joule heating in the detector element may significantly increase the temperature of the second-stage patch.

The permissible detector joule heating depends on the second-stage temperature attained in its absence and the maximum allowable detector temperature. In addition, operation of the detector at maximum or near maximum signal-to-noise ratio determines a desirable range of detector bias currents. A trade-off may therefore exist between electrical and thermal requirements. The bias current for maximum signal-to-noise ratio may produce sufficient joule heating to increase the temperature of the patch and detector to the point where detector sensitivity is decreased, thereby defeating the attempt to obtain an optimum bias current. The desirable and permissible ranges of detector bias currents cannot be set, however, until the thermal performance of the cooler is known and the electrical properties of the detector-preamplifier combination have been determined.

An initial estimate of the allowable range of detector joule heating is made in Section 4.4, following calculations of the power level ranges in the two stages of cooling. This estimate will be used to guide the design and evaluation of detector biasing and preamplifier circuitry (Section 6.2).

The first-stage patch has outside dimensions, in inches, of 13.6 by 2.15 by 0.50, from which a volume 3.375 by 1.156 by 0.050 inches is cut from the center for the second stage. The total radiating area for all outer surfaces is then 70.33 square inches. Two 1/4-inch diameter areas are used for the in-orbit support tubes, leaving a net area of 70.23 square inches. The optical opening is essentially black for radiation at the temperature of the first-stage temperature and is therefore not subtracted. The expected temperature extremes of the first-stage patch (Second Quarterly Report, Section 5.1.4) are given in Table 5 together with the corresponding radiant power levels for a black patch.

Table 5
Radiant Power Level of First-Stage Patch

Gold Emissivity	Patch Temperature	Radiant Power
0.02	86.5°K	144 milliwatts
0.086	111°K	390 milliwatts

The non-zero thickness of the second-stage patch increases its radiant power level. However, it has very little effect on the patch temperature. The increase in radiant power supplied by the sides of the patch is offset by their larger radiant coupling to the second-stage cone. As a result, previous calculations (Second Quarterly Report, Section 5.1.4) give a good estimate of the expected temperature range in the absence of significant joule heating of the detector (Section 4.4).

The dimensions, in inches, of the second-stage patch are 2.17 by 0.25 by 0.32. A 1/8-inch diameter area is used for the support tube, leaving a net surface radiating area of 2.62 square inches. The radiant power levels for a black area of this size are given in Table 6 for the temperature extremes of the second-stage patch.

Table 6
Radiant Power Level of Second-Stage Patch

Gold Emissivity	Patch Temperature	Radiant Power
0.02	64.2°K	1.63 milliwatts
0.086	79°K	3.73 milliwatts

4.4 Allowable Joule Heating of Detector

A tentative estimate of the allowable range of joule heating of the detector was made by assuming that it raises the second-stage patch temperature from 79 degrees K (corresponding to a gold emissivity of 0.086) to the range 80 degrees K to 85 degrees K. The allowable joule heating is equal to the increase in radiant power from the patch plus the decrease in conductive coupling at a fixed first-stage temperature. No change in net radiative coupling to the first-stage is produced by a change in the second-stage temperature (See First Quarterly Report, equation (91)). This may be expressed as

$$J = A_{p2}\ \sigma(T_m^4 - T_{p2}^4) + K_c\ (T_m - T_{p2}) \qquad (8)$$

where

J = joule heating of detector

A_{p2} = radiating area of second-stage patch

T_m = maximum allowable second-stage temperature

T_{p2} = second-stage temperature for $J = 0$

K_c = conductive coupling coefficient to first stage

The values of J for T_{p2} equal 79 degrees K are shown in Table 7 for maximum patch temperatures of 80 degrees K and 85 degrees K. For a detector impedance of 50 ohms, the corresponding bias currents are 2.1 and 5.4 milliamperes.

Table 7
Allowable Joule Heating of Detector

$T_{p2} = 79^oK$

T_m	J
80^oK	0.22 milliwatt
85^oK	1.48 milliwatts

5.0 OPTICAL DESIGN

The permissible aberration and longitudinal displacement (out-of-focus) were determined for each optical element. The interference filter is not included, however. Its longitudinal position is not important because it has no focusing action. A filter made in accordance with good standard practice has a negligible effect on aberrations when used in an f/8 beam. And, finally, the tolerance on tilt of the filter is large. The clear aperture of the filter, on the other hand, must be sufficient to prevent vignetting (Second Quarterly Report, Section 6.2). A complete specification for the interference filter is given in Appendix I.

5.1 Optical Aberrations and Longitudinal Displacements

The effects of two optical misalignments, decentering and tilting, were covered in Section 6.2 of the Second Quarterly Report. These misalignments plus the size of the detector element (field stop) determine the minimum clear apertures of the optical elements necessary to prevent vignetting. The third optical misalingment is longitudinal displacement or out-of-focus. Longitudinal displacements plus aberrations cause a point in the object plane to be expanded into a blur circle at the secondary image plane (detector element).

A reasonable and workable criterion is to allow the blur circle to have a diameter equal to one-half the width of the detector element (Quarterly Report I, Contract NAS5-668, 1 Sept. 1960 - 1 Dec. 1960, Section 4.1). The contributions to the blur circle have been divided among the optical elements as shown in Table 8. Aberrations and out-of-focus each contribute a blur circle of about 5 mils diameter, for a total blur circle of about 10 mils diameter or approximately one-half a detector width (0.25 mm = 9.8 mils).

Imaging the detector backwards through the optics, we see that the f/1 relay cannot be out of focus because it receives a collimated beam from the f/8 relay (See First Quarterly Report, Section 4.6 and Second Quarterly Report, Section 6.2) and forms an image of the detector in its focal plane.[1] The tolerance on placing the f/1 prime with respect to the f/1 relay is then the sum of their allowable longitudinal displacements, ± 4 mils. The longitudinal placement tolerances on the optical elements are then as given in Table 9.

---

1 A separate problem is placing the chopper wheel in the proper place, i.e., within a certain tolerance.

Table 8
Allowable Aberrations and Out-of-Focus

	Aberrations	
Element	At image plane of element	At secondary focus
f/1 Prime	1.2 mils* (0.3 mr)**	2.4 mils
f/1 Relay	1.25 mils (1 mr)	2.5 mils
f/8 Relay	< 4 mils (< 0.4 mr)	< 1 mil
Aplanat	< 1 mil	< 1 mil

	Out-of-Focus	
Element	Longitudinal along optic axis	Lateral at secondary focus
f/1 Prime	± 2 mils	± 1 mil
f/1 Relay	± 2 mils	± 1 mil
f/8 Relay	± 20 mils	± 0.6 mil
Aplanat	± 5 mils	± 2.5 mils

* mil = 1×10^{-3} inch ** mr = 1×10^{-3} radian

Table 9
Longitudinal Tolerances on Optical Elements

Element	Longitudinal Tolerance	With respect to
f/1 Prime	± 4 mils	f/1 Relay
f/1 Relay	-	-
f/8 Relay	± 20 mils	Aplanat
Aplanat	± 5 mils	Detector

6.0 ELECTRONIC DESIGN

The design of the second-stage patch depends to a large extent on the required detector package. In addition, the bias current and resultant joule heating of the detector element may significantly increase the temperature of the second stage (Section 4.4). An investigation of preamplifier and bias circuitry was therefore started to determine the electrically desirable range of bias current.

6.1 Infrared Detector

The second-stage patch was initially designed to hold a detector package similar to that presently used for the PbSe element in Nimbus High Resolution Infrared Radiometer (Contract NAS5-668). This requires the use of an overcoat or encapsulating material to protect the sensing element from atmospheric effects. At present, however, no such coating is known for Hg-Cd-Te, although an investigation is underway at Honeywell Radiation Center, Boston. The sensing element will therefore be enclosed in a space filled with dry helium or nitrogen gas and radiation admitted through a clear Irtran II (Eastman Kodak) window. This change, plus the desire of Honeywell to use an assembly similar to ones already in use, resulted in a detector package which extends beyond the height (0.32 inch) of the rest of the second-stage patch.

The detector package is shown in Figure 5, Section 2.2. The housing is made of Kovar to match the thermal expansion of the glass beads used to hermetically seal the electrical feed-throughs. This entire assembly containing a Hg-Cd-Te element will be mounted in a dewar for laboratory testing of the detector.

6.2 Preamplifier and Bias Circuitry

The Hg-Cd-Te infrared detector will require the design and evaluation of a special preamplifier. In addition to the normal preamplifier requirements of low noise, etc., this preamplifier must operate with a low impedance source (50 ohms).

A program to produce a suitable preamplifier, to measure the Hg-Cd-Te detector cell characteristics, and to determine the adequacy of a-c biasing as a substitute for electromechanical radiation chopping has been prepared. The program outline is as follows:

a. Investigation of preamplifier requirements

b. Design of a-c coupled preamplifier

c. Purchase of Perry Model 600 preamplifier

d. Preamplifier measurements and comparisons

e. Hg-Cd-Te evaluation

f. A-c biasing comparison test

Some circuit development and breadboarding has been done. We have purchased a Perry Model 600 preamplifier to verify detector measurements by Honeywell, who use this preamplifier in their test equipment.

Schematics of two preamplifier circuits presently under study are shown in Figures 10 and 11. The circuits are used with a chopped radiation signal.

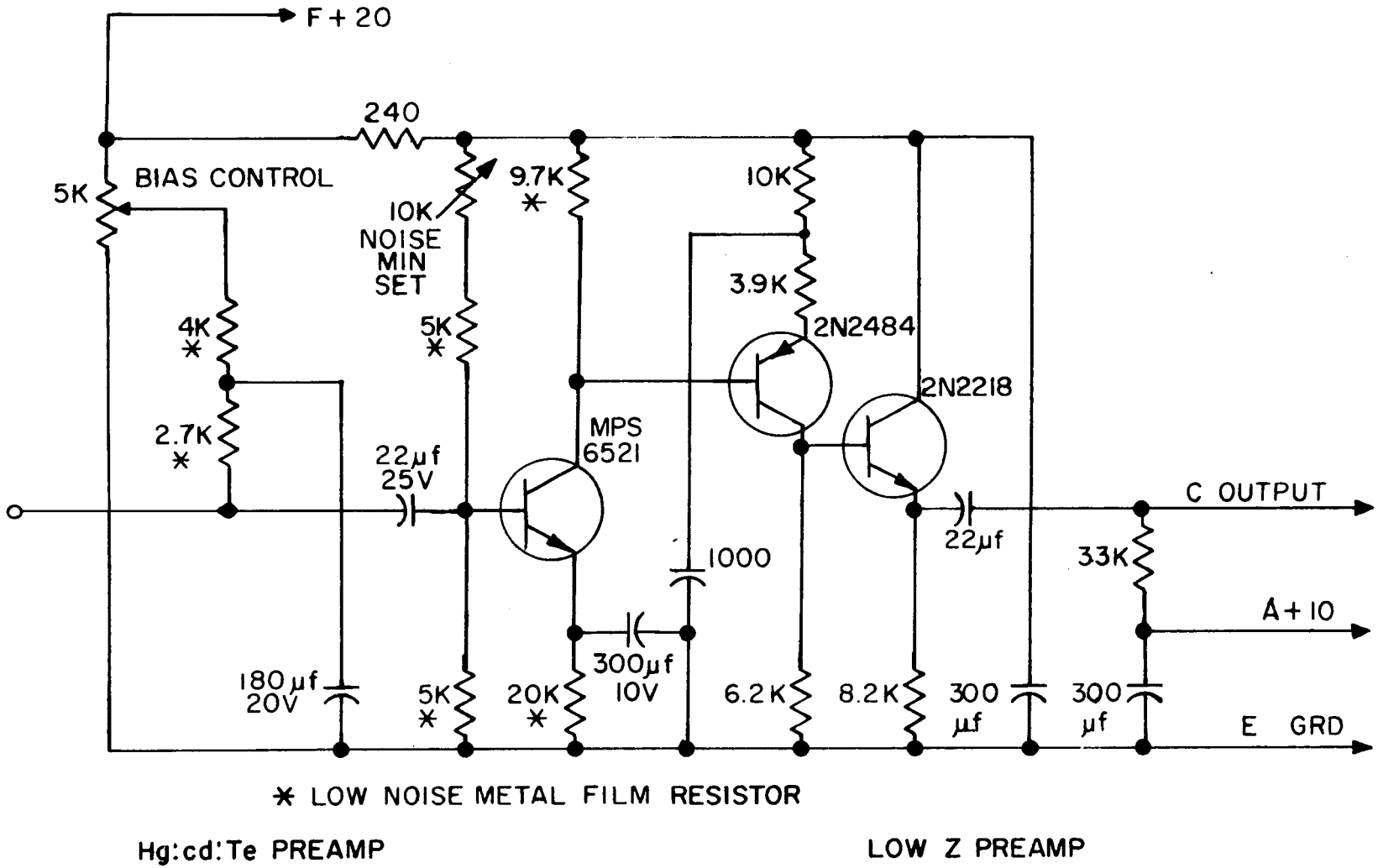

Figure 10 Low Impedance Preamplifier

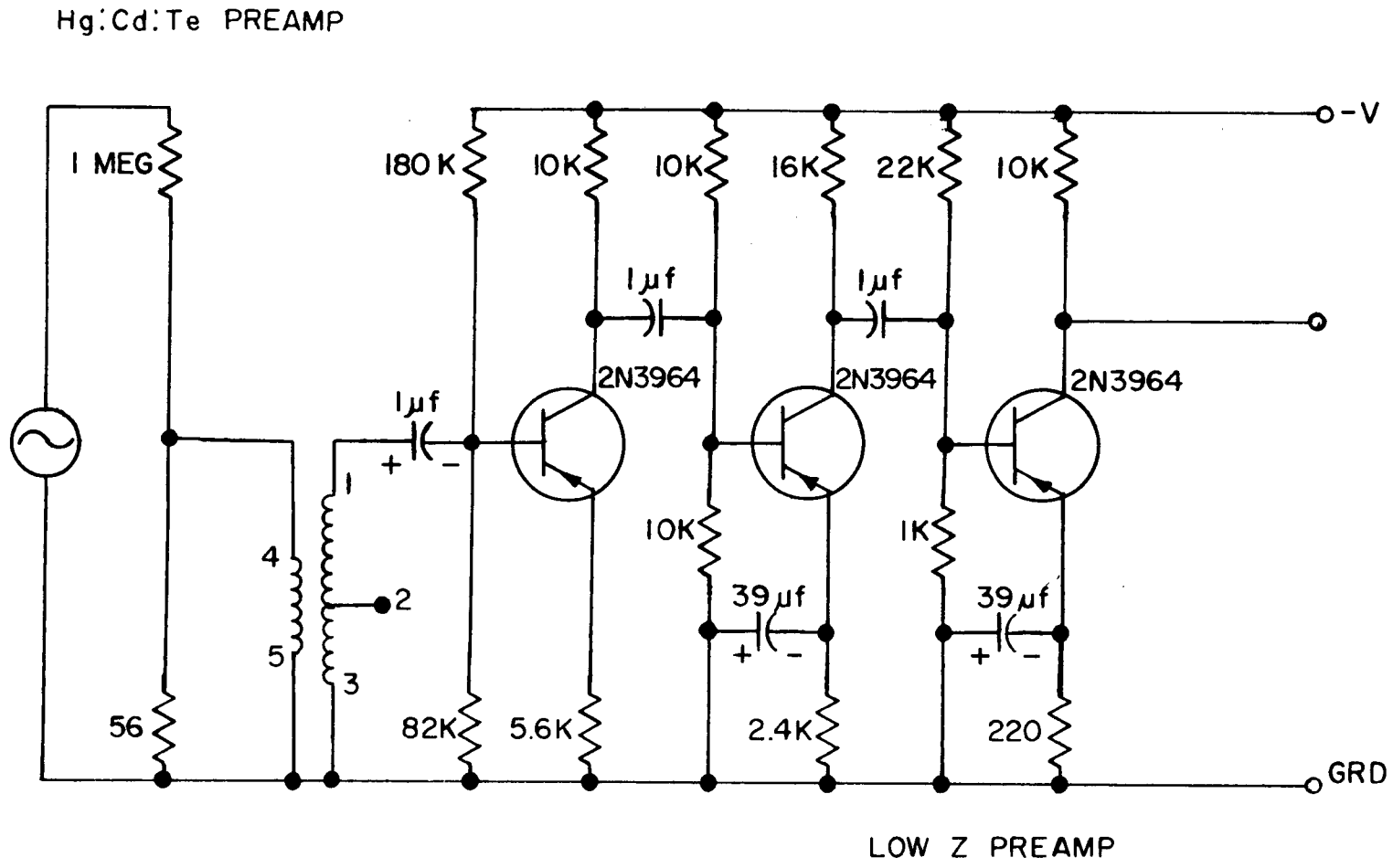

Figure 11 Transformer Coupled Preamplifier

7.0 NEW TECHNOLOGY

No items which are considered new technology according to the NASA New Technology clause of September 1964 were developed during the third quarter of the contract.

8.0 PROGRAM FOR NEXT QUARTER

The objectives of the fourth quarter effort will be to complete the test facility and begin thermal testing of the initial, single-stage model of the cooler. The space chamber will be installed[2] and mated to the helium refrigerator. The test equipment will be attached to the space chamber and the entire facility checked out. Construction of the initial cooler model will be completed and construction of a second stage begun. Time permitting, the initial model will then be tested under conditions thermally simulating outer space operation.

---

2 This was not done during the third quarter because of failure of the space chamber vendor to deliver. Delivery is presently expected in January, 1967.

APPENDIX I

SPECIFICATION FOR INFRARED BANDPASS FILTER

1.0 GENERAL

A filter for transmitting radiation in the 10.5 to 12.5 micron band for use in a spaceborne radiometer is desired. The filter will be used in conjunction with a mercury-cadmium-telluride infrared detector and must be capable of rejecting sunlight reflected from the earth's cloud cover. Because of the ozone absorption band between 9 and 10 microns, the location of the "cuton" wavelength at 10.5 microns and the slope of the "cuton" are especially important.

2.0 SPECTRAL BANDPASS

Ideally, the filter would have zero transmission from 1.7 microns to 10.5 microns, 100 percent transmission from 10.5 to 12.5 microns and zero transmission from 12.5 to 16 microns (a germanium lens will absorb radiation below 1.7 microns; the detector has negligible response to radiation of wavelengths greater than 16 microns). Actually, the filter shall have its 5 percent transmission points at 10.3 and 12.7 microns. Accuracy of location of the 5 percent transmission points shall be $\pm$ 0.1 micron. The "cuton" slope shall be 3 percent, i.e. the filter transmission from its 5 percent transmission point shall increase to 80 percent of peak transmission within 0.3 micron or less. From 10.6 microns to 12.4 microns the filter shall have an average transmission of 75 percent or more. The "cutoff" slope shall also be 3 percent, i.e. the transmission shall decrease from 80 percent of peak transmission at 12.4 $\pm$ 0.1 micron to 5 percent at 12.7 $\pm$ 0.1 microns.

3.0 BLOCKING

The transmission from 1.7 microns to 9.7 microns shall be 0.2 percent or less. From 13.4 to 16 microns the transmission shall be 0.5 percent or less.

4.0 SIZE AND QUALITY

The filter substrate shall be $0.40 \,^{+.00}_{-.01}$ inches in diameter and 0.040 inch, $\pm$ 0.005 inch in thickness. The filter coatings shall have a diameter of $0.355 \,^{+.045}_{-.000}$ inch diameter and centered on the substrate within $\pm$ 0.01 inch. Parallelism of the faces, flatness of each face, digs and scratches, etc. shall be in accordance with good standard optical practice for this type component.

5.0 ENVIRONMENT

The filter should be capable of withstanding repeated temperature cycling between 20 degrees C and -170 degrees C without appreciable change in transmission characteristics or peeling of the filter coatings from its substrate. The rate of cooling will be several hours. This temperature cycling will take place in a high vacuum chamber operating at a pressure of about 3×10^{-7} torr.

APPENDIX II

ALUMINUM SHROUD FOR COPPER COLD TARGET

The copper structure used to simulate cold space for the two-stage radiant cooler will be shielded from room temperature radiant sources by means of an aluminum shroud at about liquid nitrogen temperature. The shroud will reduce the thermal input to the outer surface of the copper members to a negligible value. The shroud will be connected to the intermediate cold exchanger of the Norelco A-20 helium refrigerator.

The approximate configuration of the aluminum shroud is shown in Figure II-1. The total temperature drop from the top of a thin side plate to the A-20 intermediate stage is about 30 degrees K. This drop is calculated below using the approach described in Appendix XII to the First Quarterly Report. The total heat load on the shroud is about 15 watts when its outer surface is covered with aluminized mylar. At this level of refrigeration, the intermediate heat exchanger will be at about 53 degrees K when the cold head is producing 60 watts at 17 to 18 degrees K; see Figure II-2. The maximum shroud temperature is then about 83 degrees K.

The shroud has a volume of about 0.2 cubic foot and weighs about 35 pounds.

We will assume that the entire heat load enters via the thin end plates by radiation from an enclosure at 300 degrees K. The shroud will be made of 1100 aluminum*, which has a thermal conductivity at ~ 80 degrees K of 2.5 watts/cm degrees K ("Cryogenic Materials Data Handbook", the Martin Co., for AF Materials Lab., WPAFB, Ohio, Aug. 1964, AD 609 562).

From Appendix XII to the First Quarterly Report, the temperature drop from the top or bottom of an end plate to its center is

$$\Delta\theta_1 = \frac{HL^2}{2K\delta} \qquad \text{(II-1)}$$

where

H = irradiance of shroud outer surface

L = length of conduction path

K = thermal conductivity

δ = thickness

---

* 99 Percent pure aluminum.

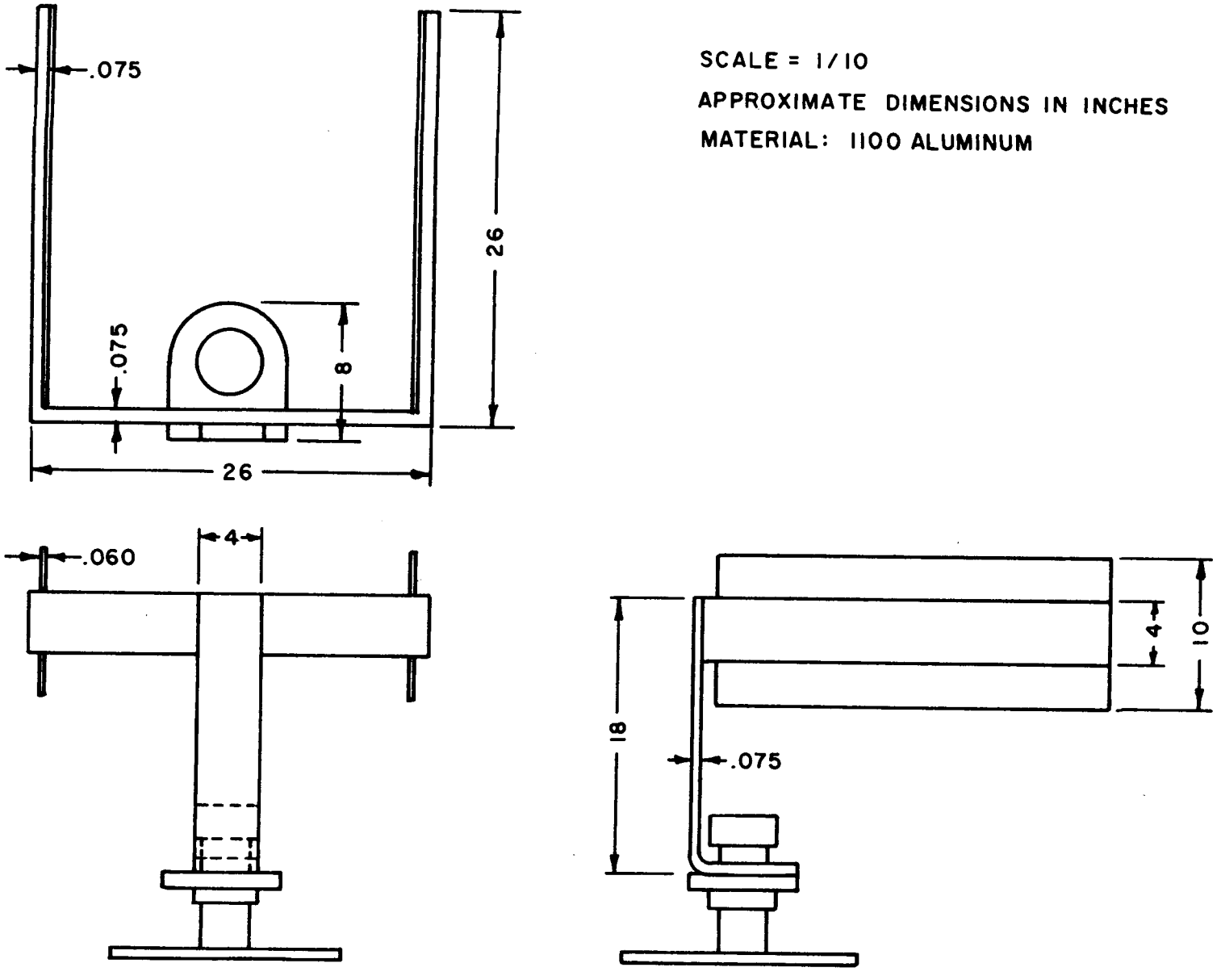

SCALE = 1/10

APPROXIMATE DIMENSIONS IN INCHES

MATERIAL: 1100 ALUMINUM

Figure II-1 Aluminum Shroud

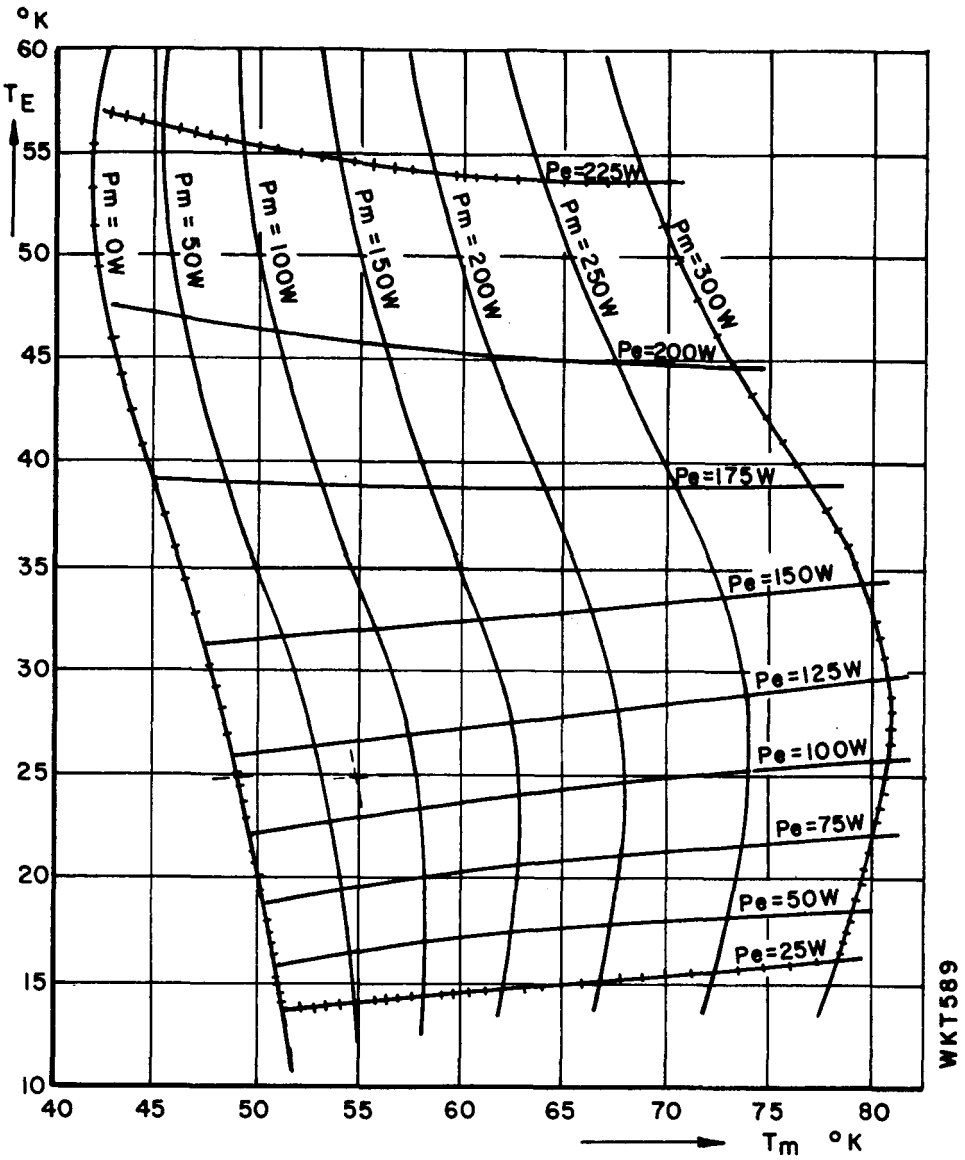

Figure II-2 Shroud Temperature Characteristics

Pm = Cold production at the intermediate cold exchanger
Pe = Cold production in the second cold exchanger
Tm = Temperature at the intermediate cold exchanger
Te = Temperature at the second cold exchanger

Example

Assuming a temperature Te of 25°K is required on the second cold exchanger (e. g. for liquifaction of a gas) and a temperature of the intermediate cold exchanger Tm of 55°K (for pre-cooling this gas). The cold output of the first cold exchanger Pm is found by interpolation between the Pm values of 50 and 100 W viz. about 70 Watt. The cold output of the second cold exchanger Pe is found by interpolation between the Pe values of 100 and 125 Watt viz. about 112 Watt.
If the cold output on the intermediate cold exchanger is zero (no pre-cooling) the production on the second cold exchanger will be somewhat higher, viz. 120 Watt.

Note: The values given in the curves are average values and may deviate 20% for different machines.

The irradiance is given by

$$H = \epsilon_s \sigma T^4 \qquad \text{(II-2)}$$

where

ϵ_s = emissivity of shroud outer surface

T = temperature of enclosure

For

ϵ_s = 0.1 (aluminized mylar)

T = 300 degrees K

we obtain

$$H = 4.6 \times 10^{-3} \text{ watts/cm}^2 \qquad \text{(II-3)}$$

Then for

L = 5 inches

ℓ = 26 inches

δ = 0.060 inch

K = 2.5 watt/cm degrees K

the temperature difference is

$$\Delta\theta_1 = 1.0 \text{ degree K} \qquad \text{(II-4)}$$

The temperature drop through the crossbar centered on an end plate is given by

$$\Delta\theta_2 = \frac{QL}{2\delta\ell K} \qquad \text{(II-5)}$$

where Q is the total power on an end plate (7.7 watts) and ℓ the width of the bar. This equation also assumes a uniform loading along the length of the bar. For

L = 26 inches

ℓ = 4 inches

δ = 3/4 inch

the temperature difference is

$$\Delta\theta_2 = 5.3 \text{ degrees K} \qquad \text{(II-6)}$$

The portion of crossbar between end plates is considered as if all the heat flux from the end plates is conducted through the cross-sectional area of the bar. The temperature drop is then

$$\Delta\theta_3 = \frac{QL}{K\,\delta\,\ell} \qquad \text{(II-7)}$$

Between an end plate and the crosspiece to the A-20, we have

L = 13 inches

δ = 3/4 inch

ℓ = 4 inches

and

$$\Delta\theta_3 = 5.2 \text{ degrees K} \qquad \text{(II-8)}$$

The crosspiece to the A-20 carries the thermal load from both end plates. The temperature drop across this member is then

$$\Delta\theta_4 = \frac{2QL}{K\,\delta\,\ell} \qquad \text{(II-9)}$$

For

Q = 7.7 watts

L = 22 inches

ℓ = 4 inches

δ = 3/4 inch

the temperature difference is

$$\Delta\theta_4 = 17.8 \text{ degrees K} \qquad \text{(II-10)}$$

The contacting interfaces also show a temperature drop, given by

$$\Delta\theta_1 = \frac{1}{h_c} \times \frac{\text{thermal load}}{\text{contact area}} \qquad \text{(II-11)}$$

For a bare contact, h_c is approximately 1.0 watt/cm^2 degree K. Between an end plate and bar, the contact area is 671 cm^2 and the temperature drop 0.012 degree K. Between the bar and crosspiece, the contact area is 103 cm^2 and the temperature drop 0.15 degree K for the thermal load of 15.4 watts. And between the crosspiece and A-20 intermediate stage, the area is 244 cm^2 and the temperature drop 0.063 degree K.

The total $\Delta\theta$ from the plates to the A-20 is then

1.0 degree K at end plate

5.3 + 5.2 = 10.5 degrees K at crossbar

17.8 degrees K at crosspiece

$$\frac{0.012 + 0.15 + 0.63 = 0.2 \text{ degree K at interfaces}}{\text{Total } \Delta\theta = 29.5 \text{ degrees K}} \qquad \text{(II-12)}$$

The A-20 intermediate stage operates at approximately 53 degrees K when 60 watts are being drawn from the cold head at 17 to 18 degrees K. The temperature in the warmest part of a shroud end plate is then ~ 83 degrees K.

APPENDIX III

SUPPORT CABLES FOR COPPER COLD TARGET AND ALUMINUM SHROUD

The copper cold target and aluminum shroud will each be suspended by four cables from a stainless steel frame attached to the space chamber (Section 3. 0). The cables will be 1/8-inch diameter 304 stainless steel, each about 6 inches in length. The average thermal conductivity of 304 stainless between 300 degrees K and 20 degrees K is 0. 102 watt/cm degree C (P. D. Fuller and J. N. McLagan in "Applied Cryogenic Engineering", Ed. by R. W. Vance and W. M. Duke, Wiley, 1962, p. 225).

The four cable suspension from the space chamber at 300 degrees K to the copper target at 20 degrees K then conducts a power of

$$4 \quad \frac{0.102 \times \pi \times 2.54 \times 280}{4 \times 64 \times 6} = 0.6 \text{ watt}$$

This is only 1 percent of the designed power load on the second cold exchanger of the helium refrigerator.

The power conducted by the four cables from the space chamber at 300 degrees K to the aluminum shroud at 80 degrees K is about

$$\frac{220}{280} \times 0.6 = 0.47 \text{ watt}$$

This is about 3 percent of the radiation load on the intermediate cold exchanger (Appendix II) and would increase its temperature a negligible amount (< 0.1 degree K).